Simulation of long-term future climate changes with the green McGill paleoclimate model: The next glacial inception

**Anne-Sophie B. Cochelin · Lawrence A. Mysak ·
Zhaomin Wang**

Abstract The multi-component "green" McGill Paleoclimate Model (MPM), which includes interactive vegetation, is used to simulate the next glacial inception under orbital and prescribed atmospheric CO_2 forcing. This intermediate complexity model is first run for short-term periods with an increasing atmospheric CO_2 concentration; the model's response is in general agreement with the results of GCMs for CO_2 doubling. The green MPM is then used to derive projections of the climate for the next 100 kyr. Under a constant CO_2 level, the model produces three types of evolution for the ice volume: an imminent glacial inception (low CO_2 levels), a glacial inception in 50 kyr (CO_2 levels of 280 or 290 ppm), or no glacial inception during the next 100 kyr (CO_2 levels of 300 ppm and higher). This high sensitivity to the CO_2 level is due to the exceptionally weak future variations of the summer insolation at high northern latitudes. The changes in vegetation re-inforce the buildup of ice sheets after glacial inception. Finally, if an initial global warming episode of finite duration is included, after which the atmospheric CO_2 level is assumed to stabilize at 280, 290 or 300 ppm, the impact of this warming is seen only in the first 5 kyr of the run; after this time the response is insensitive to the early warming perturbation.

1 Introduction

During the past 900 kyr, the evolution of the climate on orbital time scales has consisted of various quasi-periodic fluctuations, the most dramatic of which are the relatively recent 100-kyr ice age cycles (e.g., see Shackleton and Opdyke 1976; Clark and Pollard 1998). The alternation between long cold glacials and relatively short warm interglacials during the past 500 kyr is attributed to a complex set of processes involving orbital forcing and internal interactions and feedbacks in the climate system. In this paper, an Earth system Model of Intermediate Complexity (EMIC) as described in Wang Y. et al. (2005a) is used to investigate the timing of the next glacial under orbital forcing and a range of prescribed atmospheric CO_2

A.-S. B. Cochelin · L.A. Mysak (✉) · Z. Wang
Department of Atmospheric and Oceanic Sciences, McGill University, 805 Sherbrooke Street West,
Montreal, Quebec H3A 2K6, Canada
e-mail: lawrence.mysak@mcgill.ca

concentrations. Recently, the term EMIC has been introduced into the literature to describe a class of climate models that lies between simple conceptual models and comprehensive coupled atmosphere-ocean general circulation models (GCMs) (Claussen et al. 2002). In EMICs, the number of processes and/or the detail of the description is reduced for the sake of simulating feedbacks between as many components of the climate system as feasible, and in order to carry out long-term climate change runs that are beyond the scope of GCMs.

Some scientists have tried to predict future climate changes over the next millennia from analogues in the records of past climate variations. Kukla et al. (1972) suggested that the present interglacial, the Holocene, had already lasted too long (11 kyr) and hence predicted an imminent abrupt glaciation. Broecker (1998) also proposed that the present interglacial should end abruptly. However, the present interglacial may be much longer than past ones because of: (1) a rather different solar forcing in the future, and (2) the impact of anthropogenic activities. In terms of orbital forcing alone, the best analogue to the present interglacial is MIS 11 (which started around 420 kyr BP (before present)). According to recent ice core records from Antarctica, this was an exceptionally long interglacial (EPICA 2004).

Others scientists have carried out modelling studies with EMICs to determine how the long-term climate varies under natural forcing conditions. Berger et al. (1991) reviewed earlier modelling attempts to simulate future long-term climate changes under orbital forcing and a constant atmospheric CO_2 concentration of about 225 ppm (the average CO_2 level during the 100-kyr glacial cycles). The models predicted a slow cooling trend which started at 6 kyr BP and continued for the next 5 kyr. After a stable climate for over 25 kyr, there was a cold interval at around 25 kyr AP (after present) and a major glaciation at around 55 kyr AP.

Loutre and Berger (2000) ran the LLN model (an hemispheric EMIC) for the next 130 kyr under orbital forcing and constant CO_2 concentrations ranging from 210 to 290 ppm. They found that the date for the next glaciation depended critically on the CO_2 level. Moreover, for a concentration higher than 250 ppm, the LLN model simulated a melting of the Greenland ice sheet during the first 50 kyr; however, this ice sheet grew back after the glacial inception.

There have also been several model investigations in which orbital forcing has been combined with a variable atmospheric CO_2 radiative forcing. Oerlemans and Van der Veen (1984) forced a simple ice sheet model with a variable CO_2 concentration similar to that associated with the last two major ice age terminations. They predicted a long interglacial lasting another 50 kyr. Loutre and Berger (2000) ran long-term simulations of the orbitally forced LLN model with a future "natural" CO_2 variation, similar to that which occurred during the past 130 kyr. They also simulated a long interglacial lasting another 50 kyr.

Today, it is not possible to neglect the impact of human activities in the study of future long-term climate changes. The climate of the 20th century has been dominated by a warming in almost all parts of the globe. The global average surface temperature has increased by $0.6 \pm 0.2\,°C$ during this period, with the 1990s being the warmest decade (Houghton et al. 2001). Houghton et al. (2001) suggest that most of the warming of the last 50 years is due to the anthropogenically induced increase of greenhouse gases (CO_2, CH_4, N_2O and others) in the atmosphere.

If these greenhouse gases continue to increase, it is natural to ask whether anthropogenically induced warming could totally disrupt the natural long-term evolution of the climate, i.e., postpone the end of the current interglacial or even lead to a completely new climatic regime (Saltzman et al. 1993). Twelve thousand years ago, the sudden cool period called "Younger Dryas", which is generally attributed to the weakening or shut down of the ocean thermohaline circulation (THC), interrupted the warming trend after the last glacial maximum at 21 kyr BP. Model studies suggest that a continued global warming may also result in an abrupt climate change (a cooling) due to a weakening or collapse of the THC (e.g., see

Clark et al. 2002; Wood et al. 2003). The study of future climate changes thus requires the analysis of the possible competition between the natural forcing due to the orbital changes and the humanly induced radiative forcing due to increasing greenhouse gases.

Loutre and Berger (2000) ran long-term simulations of the orbitally forced LLN model with a thousand-year CO_2 scenario labelled "Global Warming", which included a rapid increase of the CO_2 concentration followed by a slow decrease. Their results showed the formation of ice sheets after 50 kyr AP; however, the ice volume was lower than the one obtained without the global warming episode. After 70 kyr AP, the evolution of the total ice volume approached the one obtained with the "natural CO_2 scenario" and the climate system was no longer sensitive to what could happen to the CO_2 over the next few centuries. Archer and Ganopolski (2005), on the other hand, used the Potsdam CLIMBER-2 model to show that if there is an anthropogenic release of 1000 GtC into the atmosphere over the next few centuries, there would not be a glaciation until at least 130 kyr AP.

The main goal of this paper is to determine possible starting dates for the next glacial by running the multi-component green McGill Paleoclimate Model (MPM) under orbital forcing and prescribed CO_2-induced radiative forcing for the next 100 kyr. The absence of a global carbon cycle in the green MPM requires us to use different prescribed scenarios for the future atmospheric CO_2 concentration. These scenarios do or do not include a global warming episode in the near future. We analyze the response of the model to these different external forcings.

The green MPM is an EMIC which has been under development at McGill University since 1992 and is continously being improved (e.g., see Wang and Mysak 2000, 2002; Wang et al. 2004; Wang et al. 2005a,c). The green MPM includes an interactive vegetation component and has successfully simulated the last glacial inception, at around 119 kyr BP (Cochelin 2004; Wang et al. 2005), and also Holocene millennial-scale natural climate changes (Wang et al. 2005b).

This paper is structured as follows. In Section 2, basic information about glacial inception, future variations in solar insolation and possible future changes in atmospheric CO_2 concentration are presented. In the next section, the green MPM is briefly described. In Section 4, the results of simulations for the short-term future climate are given; these illustrate the response of the green MPM to a warming of the climate over the next several centuries. In Section 5, the results of long-term orbitally forced simulations of the climate over the next 100 kyr with different CO_2 scenarios are presented. The conclusions are given in Section 6.

2 Future variations of the solar forcing and CO_2 concentration

2.1 The interglacial – glacial transition

The Milankovitch (1941) theory of long-term climate change states that a glaciation is initiated when the summer insolation at northern high latitudes decreases substantially and reaches very low values. However, changes in the concentrations of greenhouse gases in the atmosphere amplify the glacial inception process, through different feedbacks (e.g., see Gallée et al. 1992; Ruddiman 2003).

The solar forcing at the top of the atmosphere slowly oscillates due to changes in three astronomical parameters: the eccentricity, the obliquity and the climatic precession (see Milankovitch (1941) and the expanded explanation in Ruddiman (2001)). Milankovitch (1941) argued that the conditions to enter a glaciation were a high climatic precession (summer
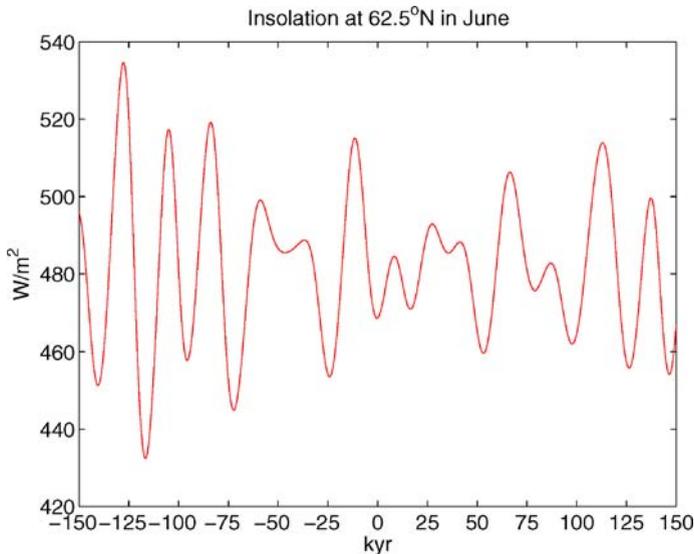
Fig. 1 Solar insolation at a high northern latitude in June, between 150 kyr BP (negative values) and 150 kyr AP (positive values), as calculated by Berger (1978). According to Milankovitch, this insolation is one of the most sensitive indicators of glacial inception

solstice at the aphelion), a high eccentricity and a low obliquity, i.e., a low insolation in summer at high northern latitudes and a low seasonal contrast.

2.2 Future variations of the solar insolation

At around 116 kyr BP, the solar insolation in June at 62.5°N approached a very low value (see Figure 1). At this time the eccentricity and climatic precession were high and the obliquity was low (Berger 1978). According to Milankovitch, the conditions were thus ideal for the initiation of a glacial period.

The evolution of the astronomical parameters over the next 100 kyr, however does not replicate the above conditions and hence it is not obvious when the next glacial inception will occur. Since the eccentricity is currently near the end of a 400-kyr cycle, its value will be low for the next 100 kyr. The future evolution of the climatic precession, which is proportional to the eccentricity, also displays very small-amplitude variations. Due to this exceptional configuration and the fact that the daily insolation is mainly a function of precession (Berger et al. 1993), the solar insolation in June at 62.5°N will vary very little for the next 100 kyr (no more than 46 Wm^{-2}), as seen on Figure 1. The minimum of this solar insolation occurring around 50 kyr AP ($\sim$ 460 W/m^2) is still notably larger than the insolation minimum characteristic of the last three glacial inceptions. Therefore the fundamental question to ask is whether this value will be low enough to trigger a glaciation.

The exceptional future evolution of the solar insolation shown in Figure 1 has very few analogues in the past 500 kyr (Berger and Loutre 1996). The best and closest analogue occurred at around 400 kyr BP, i.e., the MIS-11, an earlier interglacial period (Loutre and Berger 2000; Loutre 2003; EPICA 2004). Vettoretti and Peltier (2004) show, however, that the present-day obliquity and precession are not in phase as was the case for MIS-11. The

current orbital configuration is more similar to that during MIS-9 (around 320 kyr ago), even though the present-day value of precession is two times smaller than at MIS-9.

Because of the low-amplitude changes of the future solar insolation shown in Figure 1, the future atmospheric CO_2 level may well play an important role in long-term climate change. Berger et al. (1996) showed that the amplification of the climatic response to orbital forcing by CO_2 is especially important when the amplitude of the high northern latitudes insolation change is rather small.

## 2.3 Future changes in atmospheric CO_2 concentration

Vostok ice core data show that the CO_2 level varied between approximately 180 and 280 ppm during the past 420 kyr. Since the Industrial Revolution, the atmospheric CO_2 concentration has been undergoing an exponential increase from 280 ppm in the mid 18th century to around 380 ppm today. The recent CO_2 level is therefore unprecedented during the past 420 kyr. Moreover, Houghton et al. (2001) estimate that the future CO_2 concentration may reach 540 to 970 ppm by 2100, i.e., two-to-three times the pre-industrial concentration of 280 ppm. Recently, Archer and Ganopolski (2005) have proposed that such large CO_2 concentrations may persist for thousands of years and thus produce an extremely long interglacial.

In addition to the human-induced increase, the atmospheric CO_2 also varies because of natural exchanges of carbon between the ocean, atmosphere and land (which includes vegetation). These variations in the global carbon cycle affect and are affected by anthropogenic-induced climate change. During the Quaternary glacials, for example, CO_2 was removed from the atmosphere and absorbed by the cold oceans that had a higher solubility than at present (Beerling and Woodward 2001). Carbon was then transferred to the terrestrial biosphere from the ocean via the atmosphere during the deglaciation. Global warming will heat up the ocean and hence lower its ability to draw down large amounts of atmospheric CO_2, which will leave more of it in the atmosphere (Archer and Ganopolski 2005). Since many climate models do not have an interactive carbon cycle, they cannot calculate the emission and absorption of CO_2 by the terrestrial biosphere and ocean and thus have to be radiatively forced, in part, by a prescribed CO_2 concentration.

3 The model

The model used in this study, the green MPM, is described in Wang et al. (2004) and Wang Y. et al. (2005a). It has interactive atmosphere-land-sea ice-ocean-ice sheet-vegetation components. The land-sea configuration is shown in Figure 2. The model domain extends from 75°S to 75°N, with a north-south resolution of 5°, except across the equator where it is 10°. As seen from Figure 2, the major continents and the three main ocean basins (Atlantic, Pacific and Indian) are resolved; the Southern Ocean is represented by a well mixed region. We note that the Antarctic continent and the Arctic Ocean have been omitted. Also, by extending only to 75°N, the far northern parts of Canada and Eurasia are truncated. As a consequence, about 15 to 20% of the land area which can support ice sheet growth is missing in the model.

The MPM is a sectorially (zonally) averaged model for the atmosphere, ocean, sea ice and land surface. However, over the continents in the latitude band 30–75° N, the sectorially averaged atmospheric variables of surface air temperature (SAT), precipitation (P) and surface specific humidity (SSH) are physically downscaled in order to get their values on a five degree latitude-longitude grid (see Wang and Mysak 2002 for details). These gridded variables are
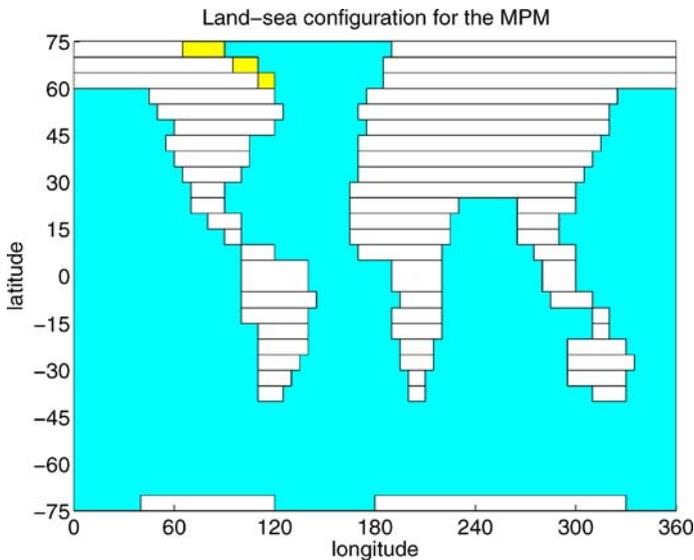
Fig. 2 Land-sea configuration for the MPM (the yellow grids correspond to Greenland)

then used to force the 2-D vertically integrated dynamic isothermal ice sheet model of Marshall and Clarke (1997), which has a horizontal resolution of $0.5° \times 0.5°$ and an ice temperature of $-5°C$. Further details on how the ice sheet model is coupled to the other components of the MPM are given in Wang and Mysak (2002). However, in contrast to the case in Wang and Mysak (2002), the Greenland ice sheet is now explicitly resolved in the green MPM, being located in the western half of the North Atlantic as part of the ice sheet model, but attached to the North American continent for the purpose of coupling it to the other components of the MPM.

The vegetation component of the green MPM originates from VECODE (VEgetation COntinuous DEscription; Brovkin et al. 2002). In VECODE, vegetation is classified into three plant function types–trees, grass and desert. The annual P, annual mean SAT and growing degree day index simulated by the MPM are used to force VECODE and to produce a vegetation cover for the corresponding climate.

In order to incorporate the biogeophysical (vegetation-albedo) feedback into the geophysical MPM, a new land surface scheme was also introduced (Wang Y. et al. 2005a). It is adapted from BATS (Biosphere-Atmosphere Transfer Scheme) (Dickinson et al. 1993) and MOSES 2 (Cox et al. 1999). The resulting two major improvements to the green MPM are (1) the parameterization of the seasonal cycle of terrestrial vegetation, and (2) the calculation of a seasonal land surface albedo by using the fractions of trees, grass and desert given by VECODE, the effective snow fractions and the seasonal leaf area index for trees. In the version of the model used here, evapotranspiration is neglected.

In the green MPM, the solar energy disposition (SED) (i.e., the redistribution of the incident short wave radiation) has been modified to describe more accurately the radiative processes and interactions between the ground, atmosphere and space. The new SED scheme is described in Wang et al. (2004).

In order to validate the model, many experiments have been done to simulate past, present-day (i.e., pre-industrial) and short-term future climates. When forced by variable

insolation (Berger 1978) and Vostok-derived atmospheric CO_2 levels, the green MPM has been able to simulate the last glacial inception, and the subsequent buildup of huge ice sheets over North America and Eurasia during the glacial period (Cochelin 2004; Wang Z. et al. 2005). Due to the addition of vegetation, more realistic ice volumes and ice sheet distributions have been simulated than obtained by Wang and Mysak (2002), although the total ice sheet volume is still less than observed due to the northern boundary of the MPM being at 75°N. The equilibrium and transient responses to a future CO_2 doubling have also been simulated by the geophysical MPM (Wang and Mysak 2000) in Petoukhov et al. (2005). The results which were obtained by the geophysical MPM (with a 1-D isothermal ice sheet model and without vegetation and the new SED scheme), were within the range of GCM results and compared favorably with seven other EMIC results.

4 Simulation of short-term future climate changes

We first carried out various short-term simulations with an increasing atmospheric CO_2 concentration, followed by a stabilization of the CO_2. The objective was to see if the green MPM was able to respond sensibly to short-term modifications in the CO_2 forcing, i.e., in a manner similar to the response of GCMs to global warming scenarios.

4.1 The canonical $2 \times CO_2$ experiment

As mentioned at the end of Section 3, in Petoukhov et al. (2005), the geophysical MPM and seven other EMICs were run to simulate the response of the climate to the doubling of atmospheric CO_2 concentration. The scenario used for the atmospheric CO_2 forcing started at 280 ppm and then consisted of a monotonic increase of CO_2 concentration at a rate of 1% per year compounded for the next 70 years; this was followed by a stabilization at the 560 ppm level over a period longer than 1500 years.

With orbital forcing as calculated by Berger (1978), we ran the green MPM with the new SED scheme for 5000 years, starting with the pre-industrial value of CO_2 at year 1800 (280 ppm) followed by the same scenario for the atmospheric CO_2 concentration used in Petoukhov et al. (2005): this is the "equilibrium $2 \times CO_2$" run. We then compared the characteristics of the climate at the end of the equilibrium $2 \times CO_2$ run with those of the climate at the end of the equilibrium $1 \times CO_2$ run (the model run for 5000 years with a constant CO_2 concentration of 280 ppm). The surface air temperature and outgoing longwave radiation flux were both greater for the equilibrium $2 \times CO_2$ run because of the CO_2-induced warming. The difference was even greater at high latitudes, and particularly at high southern latitudes during the Southern Hemisphere winter (JJA) (figure not shown). We believe the latter is due to the melting of sea ice in the Southern Hemisphere and the strong ice-albedo feedback. There was a particularly noticeable decrease of the albedo in the high southern latitudes during austral summer (figure not shown). Our results also show an increase of precipitation near the equator and in subpolar and high-latitude regions (figure not shown), the latter being likely due to an increase of the meridional poleward moisture transport.

We next compared our equilibrium $2 \times CO_2$ results, at the end of 1500 years, with those obtained by the geophysical MPM and presented in Petoukhov et al. (2005). The green MPM simulated a larger SAT increase in high northern latitudes, especially in summer (4.5 °C, versus 2.9 °C in Petoukhov et al. 2005). The fact that we have added vegetation in the green MPM contributed to the decrease of the surface albedo. A further comparison of our results with those from the geophysical MPM (see Petoukhov et al. 2005), for the same doubling
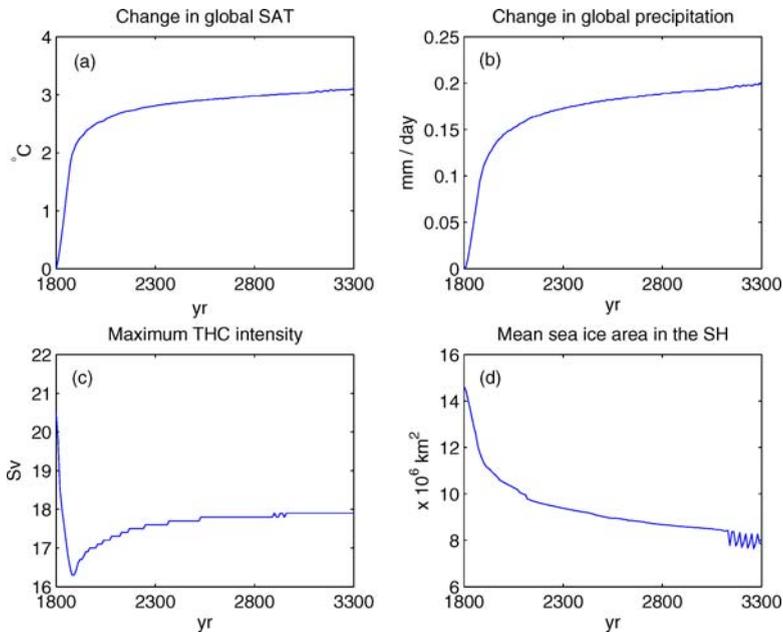
Fig. 3 Time series of the changes (equilibrium $2 \times CO_2$ run minus equilbrium $1 \times CO_2$ run) in annual mean global SAT (a), and precipitation (b) simulated by the green MPM. Time series of the evolution of the maximum THC intensity (c), and mean sea ice area in the Southern Hemisphere (d), for the equilibrium $2 \times CO_2$ run

of CO_2, shows that the presence of vegetation leads to an increase in the energy absorbed by the climate system at higher northern latitudes in summer. Our results indicated that the precipitation changes simulated by the green MPM were generally larger than those simulated by the geophysical MPM (Petoukhov et al. 2005), due to the vegetation–temperature feedback (figure not shown).

We now discuss the transient behaviour of the simulations. Figure 3a shows the difference in the global SAT between the equilibrium $2 \times CO_2$ and $1 \times CO_2$ runs over the first 1500 years of the simulations. We observe that the doubling of the CO_2 level causes the SAT to increase rapidly by $1.8\,°C$ during the first 70 years of the run; the global SAT change then slowly reaches a plateau of $3.1\,°C$ (versus $2.9\,°C$ for the geophysical MPM) after 1500 years. This increase lies right in the middle of the range of $1.5\,°C$ to $4.5\,°C$ temperature increase obtained by a number of atmospheric models coupled to a simple slab ocean for a double CO_2 climate (Le Treut and McAvaney 2000). After 110 years of simulation, we note that the global SAT increased by $2.2\,°C$, which lies in the range of 1.4 and $5.8\,°C$ increases simulated over the period 1990–2100 by a number of GCMs using the CO_2 scenarios from the SRES (Houghton et al. 2001). Like the SAT, the precipitation also shows an increase, by an amount of 6% after 1500 years (Figure 3b).

Figure 3c shows a strong reduction (-4 Sv) of the maximum strength of the THC during the first 100 years of the equilibrium $2 \times CO_2$ run, followed by a progressive increase. However, the THC intensity never returns to its initial value but asymptotes at 1500 yr to a value that is 2.6 Sv lower. This final decrease of the THC strength is quite a bit larger than the 1.8 Sv decrease obtained with the geophysical MPM (Petoukhov et al. 2005). The reduction of the North Atlantic Deep Water (NADW) formation rate associated with the slow down of the THC is caused by a decrease in the density of the high northern latitude surface waters.

The latter is due to a warming of the high latitude surface waters, as well as a freshening of these waters due to an enhanced high-latitude freshwater flux (increased precipitation and runoff) into the ocean. Manabe et al. (1991) and Manabe and Stouffer (1994) also obtained a weaker THC (less than half of its original value) by using the same CO_2 scenario with a coupled atmosphere-ocean GCM .

Finally, we observe an initial rapid decrease of the sea ice area in the Southern Hemisphere during the first 70 years of the equilibrium $2 \times CO_2$ run (Figure 3d). This is then followed by a slower decrease with the sea ice area, which reaches an equilibrium value that is 54% lower than the initial value.

4.2 Global warming experiment

Rahmstorf and Ganopolski (1999) studied global warming scenarios with an atmosphere-ocean-sea ice model of intermediate complexity. They ran the model for 1200 years, with a global warming scenario in which the atmospheric CO_2 concentration starts at 280 ppm in year 1800, slowly rises for 200 years and then rapidly increases to 1200 ppm in the 22nd century; after this, the concentration slowly declines to 395 ppm in year 3000 (see Figure 2a in Rahmstorf and Ganopolski 1999). After 350 years, they obtained a large decline in the strength of the THC, which was caused by warmer and fresher surface waters in the North Atlantic. Their results also showed that although the THC intensity finally recovered, it never returned to its initial value.

The objective of this second short-term experiment is to determine whether the green MPM is also able to respond to a quick and intense global warming episode similar to that used by Rahmstorf and Ganopolski (1999). We ran the MPM for 1200 years, from year 1800 to 3000 under orbital forcing (Berger 1978) along with the following scenario for the CO_2 concentration: the CO_2 level increases slowly from 280 ppm at 1800 to 370 ppm at 2000, and then rapidly reaches a maximum value of 1200 ppm in 2150. The increase of the CO_2 concentration follows the IS92e IPCC (Intergovernmental Panel on Climate Change) scenario, i.e., the scenario with the fastest and largest increase of CO_2. The CO_2 concentration then slowly decreases, with an e-folding time of 150 years, and reaches an equilibrium value of 395 ppm around year 3000. The pattern for the decrease of CO_2 is based on the assumption that fossil fuel use will slow down and eventually cease around year 2200, and that the ocean and the terrestrial biosphere will slowly absorb some of the CO_2 gas remaining in the atmosphere, resulting in an equilibrium concentration of 395 ppm in year 3000 (Rahmstorf and Ganopolski 1999).

From Figures 4a and 4b we note that the global SAT and precipitation changes follow quite closely the CO_2 concentration scenario. Thus, as compared with the equilibrium $1 \times CO_2$ run, the SAT and precipitation increase quite rapidly until roughly 2200, with the maximum SAT change being 4.8 °C and the maximum change in precipitation being 0.27 mm/day (i.e., an 8% increase). The SAT and precipitation for the global warming scenario then decrease slowly and asymptote to values that are still greater than the pre-industrial values (by 1.8°C for the SAT, and by 0.12 mm/day for the global precipitation). From Figures 4c and 4d we see that the maximum THC intensity and the mean sea ice area in the Southern Hemisphere first decrease rapidly until just before 2200 (by 6 Sv for the THC and by 6.8×10^6 km^2 for the sea ice area). Then, the THC intensity and sea ice area rebound toward the starting values, but still remain lower than the pre-industrial values (by 1.4 Sv for the THC and by 4.8×10^6 km^2 for the mean sea ice area). Our results are quite similar to those obtained by Rahmstorf and Ganopolski (1999).
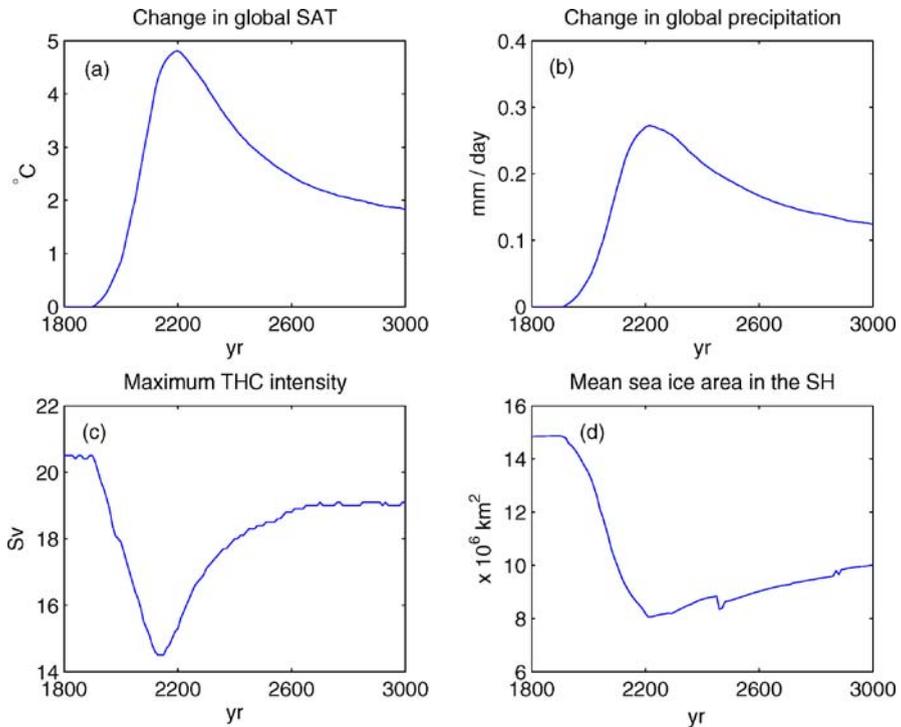
Fig. 4 Time series of the changes in annual mean global SAT (a), and precipitation (b) simulated by the green MPM for the global warming scenario introduced by Rahmstorf and Ganopolski (1999). Time series of the evolution of the maximum THC intensity (c), and mean sea ice area in the Southern Hemisphere (d), for the same global warming scenario

The above two sets of experiments show that the green MPM is able to respond to rapid changes of the CO_2 concentration. The model successfully simulates a warming of the climate, whose peak global temperature is in good agreement with the results of other EMICs and GCMs. We wish now to use the green MPM to investigate the long-term natural evolution of the climate under constant atmospheric CO_2 levels and the long-term response of the climate to future rapid changes of the CO_2 concentration induced by anthropogenic activities.

5 Simulation of long-term climate changes for the next 100 kyr

In order to produce projections for the future climate, the green MPM was run for 100 kyr, using a variety of CO_2 scenarios, orbital forcing starting in year 1950 (Berger 1978), and starting with year 1950 conditions for the ice sheets (i.e., the 1950 AD Greenland ice sheet only, as there is no Antarctic region in the model). The first set of simulations was run under various constant atmospheric CO_2 levels. In the second set of simulations, the atmospheric CO_2 concentration rapidly increases and then slowly decreases until the CO_2 level is stabilized to various levels shortly after 1 kyr AP. For the remaining 99 kyr, the atmospheric CO_2 concentration remains constant. This variation in atmospheric CO_2 represents the inclusion of an episode of global warming superimposed on the constant CO_2 scenario. In both sets of experiments the model was run with an interactive ice sheet component.
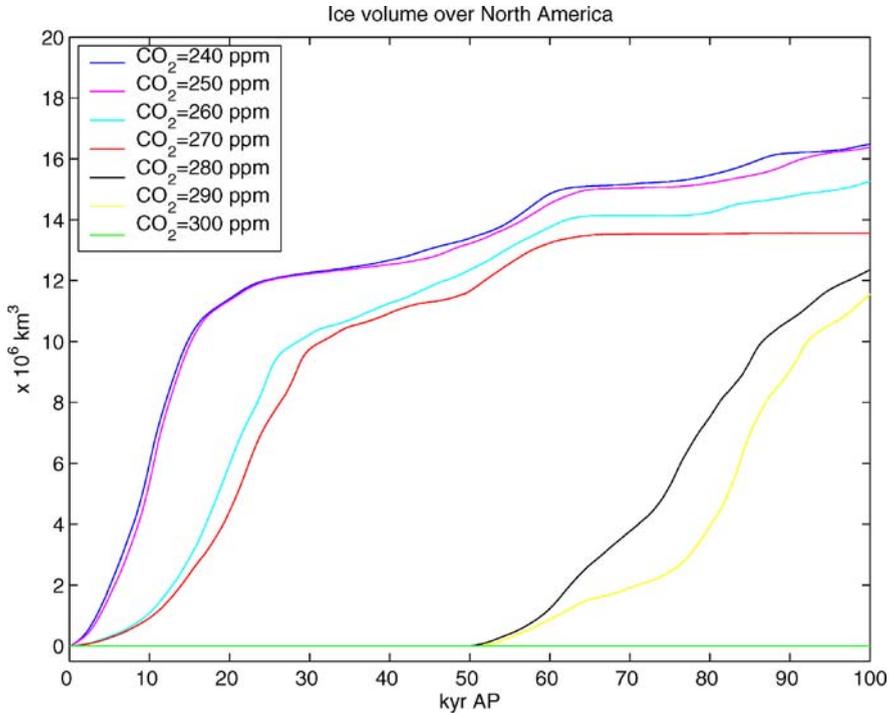
Fig. 5 Ice volume growth simulated by the green MPM over North America for the next 100 kyr, with constant CO_2 scenarios ranging from 240 ppm (blue) to 300 ppm (green). Note: Here and in Figures 6–10, AP in the time axis means after 1950

5.1 "Natural" evolution of the climate under constant CO_2 concentration

Figure 5 shows the time series of the ice volume growth obtained over North America in the first set of experiments (atmospheric CO_2 concentrations of 240, 250, 260, 270, 280, 290 and 300 ppm). Figure 6 illustrates the evolution of the maximum intensity of the THC for these experiments, and Figure 7 portrays the tree and desert fraction changes averaged over the high northern latitudes.

5.1.1 Ice volume

From Figure 5 we see that, depending on the CO_2 level, there are three possible types of evolution for the ice volume: an imminent glacial inception, a glacial inception in 50 kyr, or no glacial inception during the next 100 kyr. Mathematically speaking, the climate system passes through two thresholds for glaciation as the atmospheric CO_2 is increased.

For CO_2 concentrations less than or equal to 270 ppm, the climate enters into a glacial period fairly quickly. This is consistent with the results of Loutre and Berger (2000), who also simulated an imminent glacial inception for a CO_2 concentration of 210 ppm. Ice starts to build up in the west of the high North American latitudes and then slowly expands eastward and southward (figure not shown). The Laurentide Ice Sheet, however, starts to build up later. For a CO_2 level of 270 ppm, the ice volume reaches a plateau at around 50 kyr AP, while it continues to increase for lower CO_2 levels (Figure 5). The evolution of the ice volume
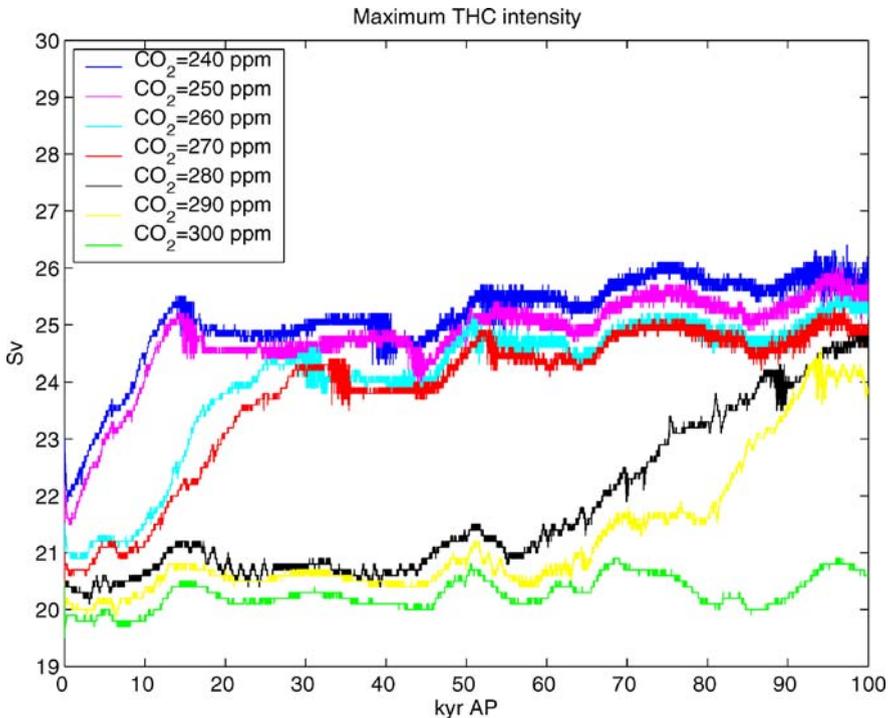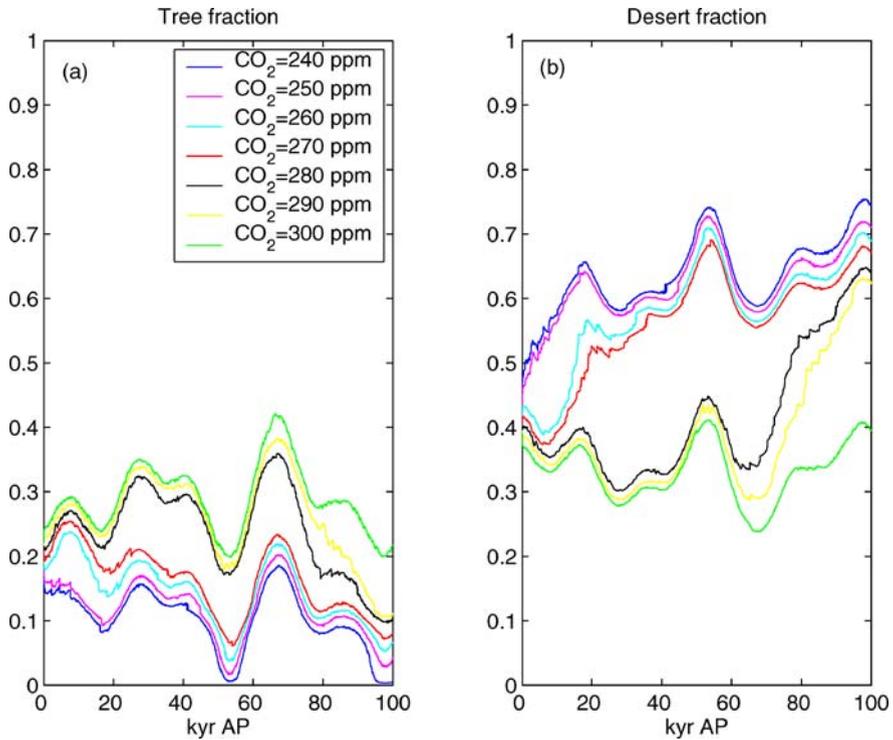
Fig. 6 Maximum THC intensity simulated by the green MPM for the next 100 kyr, with constant CO_2 scenarios: 240 ppm (blue), 250 ppm (magenta), 260 ppm (cyan), 270 ppm (red), 280 ppm (black), 290 (yellow) and 300 ppm (green)

increase is thus CO_2-dependent, with a larger and more rapid ice sheet buildup for lower CO_2 levels. The ice volume after 100 kyr ranges between 13.6 and 16.5×10^6 km^3.

For CO_2 concentrations between 280 and 290 ppm, the green MPM simulates a glacial inception in 50 kyr. Thus for some CO_2 value between 270 and 280 ppm, the first threshold for glaciation is crossed. The rate of increase of the ice volume, after this threshold is crossed, is again CO_2-dependent. For a concentration of 280 ppm, we observe a fairly linear increase of the ice volume, whereas for a CO_2 level of 290 ppm the green MPM first simulates a slow buildup of ice sheets for about 25 kyr, and then a more rapid buildup. For both CO_2 levels, the ice sheet first builds up over northwestern Canada and then expands eastward and southward (figure not shown). The appearance of the Laurentide Ice Sheet is CO_2-dependent, however: the higher the CO_2 concentration, the later the Laurentide Ice Sheet is formed.

Finally, for concentrations greater than or equal to 300 ppm, there is no glacial inception for the next 100 kyr (see green line in Figure 5). Thus there is a second threshold for glaciation between 290 and 300 ppm.

For the six runs (with constant CO_2 levels varying between 240 and 290 ppm), we observe an ice buildup over North America that is comparable in volume to that after the last glacial inception (Wang et al. 2005). In contrast to Wang et al. (2005), we do not obtain any ice sheet formation over Eurasia in the next 100 kyr, for CO_2 concentrations higher than 260 ppm. The Greenland ice volume (not shown) varies only slightly, depending mainly on the variations of the solar insolation and the precipitation at high latitudes. The simulated present-day (i.e., 1950 AD) value of the global SAT for a CO_2 concentration of 300 ppm is 0.8 °C higher than

Fig. 7 Tree (a) and desert (b) fractions averaged between 60 and 75°N simulated by the green MPM for the next 100 kyr, with constant CO_2 scenarios: 240 ppm (blue), 250 ppm (magenta), 260 ppm (cyan), 270 ppm (red), 280 ppm (black), 290 (yellow) and 300 ppm (green)

that for a concentration of 240 ppm. The global SAT and high northern latitude SAT start to decrease quite rapidly after the time of the glacial inception, due to the ice-albedo feedback and vegetation-albedo feedback.

Ice cores from the Antarctic (e.g., see Indermühle et al. 1999; Petit et al. 1999) show that the atmospheric CO_2 concentration was around 280 ppm during pre-industrial times. Moreover, due to anthropogenic activities, the value of the CO_2 concentration is 380 ppm today and is expected to increase in the next one or two centuries. It is thus very plausible that the CO_2 concentration will be greater than 280 ppm during the future millennia. The imminent glacial inception, as simulated by the MPM for concentrations less than or equal to 270 ppm, is thus not a likely scenario. Kukla et al. (1972) simulated an imminent glaciation because they did not take into account the natural variations of CO_2, and were running models with an average CO_2 concentration of 225 ppm.

5.1.2 Thermohaline circulation

The evolution of the maximum THC strength for the seven constant CO_2 runs (Figure 6) shows an overall pattern similar to that for the ice volume. In the cases where a glacial inception occurs during the next 100 kyr, the long-term increase of the strength of the THC above that at the beginning is around 4 Sv. It is also interesting to note, for the whole duration of the 300 ppm CO_2 run, the existence of a quasi-periodic 20-kyr oscillation in the THC strength,

with peak-to-peak changes of about 1 Sv. This signal is presumably due to the precessional component of the orbital forcing. These low-amplitude fluctuations also seem to be present in parts of the other CO_2 runs, but they are less visible when there is an increasing trend in the THC strength. Thus the oscillations are quite clearly seen in the 240, 250, 260 and 270 ppm runs after 30 kyr AP, and in the 280 and 290 kyr ppm runs before 60 kyr AP. During the time of rapid ice sheet buildup, the maximum strength of the THC seems to depend strongly on the ice volume evolution, and the influence of the 20-kyr precessional signal is much smaller. One possible explanation for these low-amplitude oscillations may be the orbitally forced changes in Greenland ice volume and the northern hemisphere precipitation that would modify the freshwater input at high latitudes and hence the strength of the THC.

5.1.3 Vegetation

Since ice appears first at high northern latitudes during glacial inception, it is expected that the changes in vegetation (trees and desert, in particular) would be more pronounced at these latitudes, where the vegetation responds mainly to temperature changes. Figures 7a and 7b illustrates the evolution of the tree and desert fractions, averaged between 60 and 75 °N. The tree and desert fractions averaged between 30 and 75 °N (not shown) have similar evolutions to those seen in Figure 7; however, the amplitudes of the variations are smaller.

At the start of the runs, we observe that the higher the CO_2 level, the higher the tree fraction (Figure 7a) and the lower the desert fraction (Figure 7b). A higher CO_2 concentration gives a warmer climate, and this induces an extension of the tree area and a decrease of the desert area, especially at high northern latitudes. For the next 100 kyr, the evolution of the tree fraction curves follows closely the high northern latitude summer solar insolation variations (see Figure 1), while the evolution of the desert fraction curves is opposite in phase to the solar insolation variations. After the time of a glacial inception and the subsequent buildup of huge ice sheets, there is however a superimposed trend on the tree and desert fractions: it is decreasing for the tree fraction and increasing for the desert fraction (e.g., see the curves for the 240, 250, 260 and 270 ppm CO_2 runs). As the ice sheets build up, the climate cools down, and this induces a progressive decrease of the tree area and an increase of the desert area. For a CO_2 concentration of 300 ppm, this decreasing (increasing) trend in the tree (desert) fraction is not observed since there is no glacial inception for the next 100 kyr.

To summarize, this first set of model runs shows the existence of two thresholds for glaciation with constant atmospheric CO_2. For concentrations of 270 ppm and lower, the green MPM simulates an imminent glaciation over North America. For concentrations between 280 and 290 ppm, the green MPM simulates a glacial inception in ~50 kyr. For concentrations of 300 ppm and higher, however, there is no ice sheet buildup during the next 100 kyr. The close proximity of the thresholds illustrates the high sensitivity of the green MPM to the CO_2 level in the atmosphere. The variations of the THC and the tree and desert fractions we also found to be clearly influenced by the occurrence of the glacial inception. The THC and vegetation seem to amplify the ice sheet buildup at high latitudes, but not to cause the glaciation.

5.2 Constant CO_2 concentration after an episode of global warming

In the second set of the 100-kyr simulations (which started in year 1950), we included a global warming episode during the first 1200 years of the run, similar in profile to that described in Section 4.2. During the first 150 years, the CO_2 concentration rises to 370 ppm from a starting value of 280 ppm, and then during the next 200 years it rises rapidly to a value of 1200 ppm. After this 350-year period, it decreases slowly for 850 years, until it reaches a
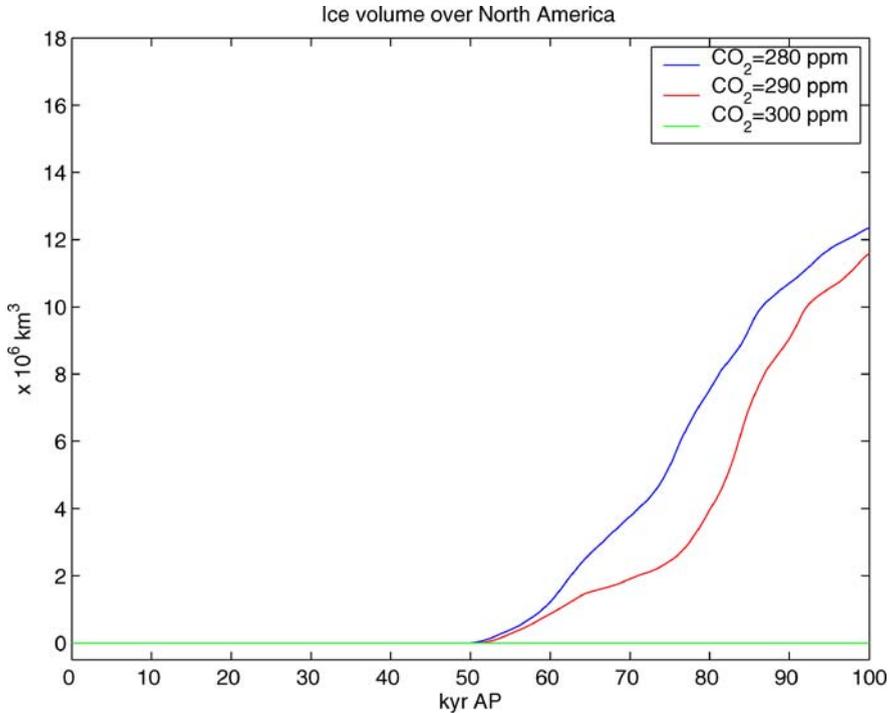
Fig. 8 Ice volume growth over North America simulated by the green MPM for the next 100 kyr, with a global warming episode followed by a constant CO_2 scenario of 280 ppm (blue), 290 ppm (red) and 300 ppm (green) after 1.2 kyr

constant value (see Figure 5.8 in Cochelin 2004). The CO_2 concentration then remains at this "equilibrium" value for the remainder of the 100-kyr run. Runs were done for three equilibrium values: 280, 290 and 300 ppm; in each case, the ice volume growth, intensity of the THC, and vegetation and desert fractions were analyzed.

5.2.1 Ice volume

Figure 8 shows the evolution of the ice volume over North America for the three CO_2 equilibrium values. We again observe the existence of a threshold for glaciation. For CO_2 concentrations of 290 ppm or less, there is a glacial inception at 50 kyr AP. For CO_2 concentrations of 300 ppm or more, the green MPM does not simulate any glacial inception for the next 100 kyr. The threshold value (for the supression of glaciation) is between 290 and 300 ppm and is therefore presumably very close to the one obtained in Section 5.1. Thus the addition of an initial global warming episode did not modify the CO_2 level over which no glacial inception will occur. These results on long-term glacial inception are consistent with those of Archer and Ganopolski (2005) who found that the Potsdam CLIMBER-2 model simulated a glacial inception 50 kyr AP for an anthropogenic release of 300 GtC (which results in a long-term atmospheric CO_2 concentration of just under 300 ppm), and no glacial inception for over 100 kyr AP when the anthropogenic input is 1000 GtC (which results in a long-term atmospheric CO_2 level of just over 300ppm) (see their Figure 3).

The Greenland ice volume in the model varies only slightly over the next 100 kyr in the presense of a global warming episode. The green MPM does not simulate any significant melting of the Greenland ice sheet, which is in contrast to what is suggested by Gregory and Huybrechts (2004) for a sustained global warming of more than 2.7 °C. Due to increased precipitation at high latitudes, the green MPM simulates a slight increase of the Greenland ice volume during the first 1200 years. We note, however, that the green MPM has too coarse a resolution to resolve the Greenland ice sheet satisfactorily. That might explain why our results are quite different from those of Loutre and Berger (2000), who obtained an almost complete melting of the Greenland ice sheet for their long-term simulations which included a global warming episode. However, Loutre (2003) has noted that one of the weaknesses of the LLN model was the too-frequent melting of the Greenland ice sheet during the warm interglacials. Finally, Letreguilly et al. (1991) showed that with a 3-D ice sheet model, the Greenland ice sheet might be vulnerable to a climate warming, due to the presence of large ablation areas along the ice-sheet edges. The ice sheet would disappear totally if a temperature increase of $6°C$ was sustained over Greenland for 20 kyr, or if a $8°C$ increase was sustained for 5 kyr. Using the scenario described earlier, with a CO_2 equilibrium value of 300 ppm, the green MPM only sustains a large increase of global temperature (up to 4.8°C) over a few centuries. Once the SAT is stabilized, its value is only 0.5°C higher than the initial value, and this does not trigger a melting of the Greenland ice sheet.

5.2.2 Thermohaline circulation

As seen on Figure 9a, the maximum strength of the THC in each case first rapidly decreases in response to the relatively large CO_2 increase and the subsequent general warming of the climate. The THC strength then rapidly increases until about 1200 years AP, after which time it slowly decreases. For a CO_2 concentration of 280 ppm, the THC intensity finally returns close to its initial value after around 10 kyr AP. This is not the case for the other two CO_2 concentrations. The THC strength at around 10 kyr AP is about 0.7 Sv (0.3 Sv) lower than the initial value for the case of a CO_2 equilibrium value of 300 ppm (290 ppm) (see Figure 9a). The evolution of the THC strength for the rest of the 100-kyr run (Figure 9b) then follows the ice volume curve and increases after 50 kyr AP for CO_2 levels of 280 and 290 ppm due to the cooling of the climate and the decreased river runoff generated by the buildup of ice sheets. Figure 9b shows, for the 280, 290 and 300 ppm CO_2 cases, quite similar evolutions of the THC strength to the ones seen in Figure 6, after 1200 yr AP.

5.2.3 Vegetation

Figures 10a and 10b illustrate the evolution of the high northern latitude tree and desert fractions for the three CO_2 runs. We observe first a rapid increase (decrease) and then a rapid decrease (increase) of the tree (desert) fraction; the tree fraction time series follows the prescribed variations of the CO_2 concentration and the SAT, whereas the desert fraction time series varies inversely with these quantities. The tree (desert) fraction increases (decreases) rapidly when the climate warms up and then decreases (increases) relatively quickly when the climate returns to its initial state. These rates of change for the tree and desert fractions are comparable to what have been simulated and observed for the pre-industrial Holocene (e.g., see Wang Y. et al. 2005b), and thus the rates of change are deemed to be reasonable. After these large-amplitude variations, the tree and desert fractions oscillate about a mean level, in a manner similar to those described in Section 5.1.3. Before the time of the glacial inception, the tree (desert) fraction evolution is similar (opposite) to the solar insolation variations.
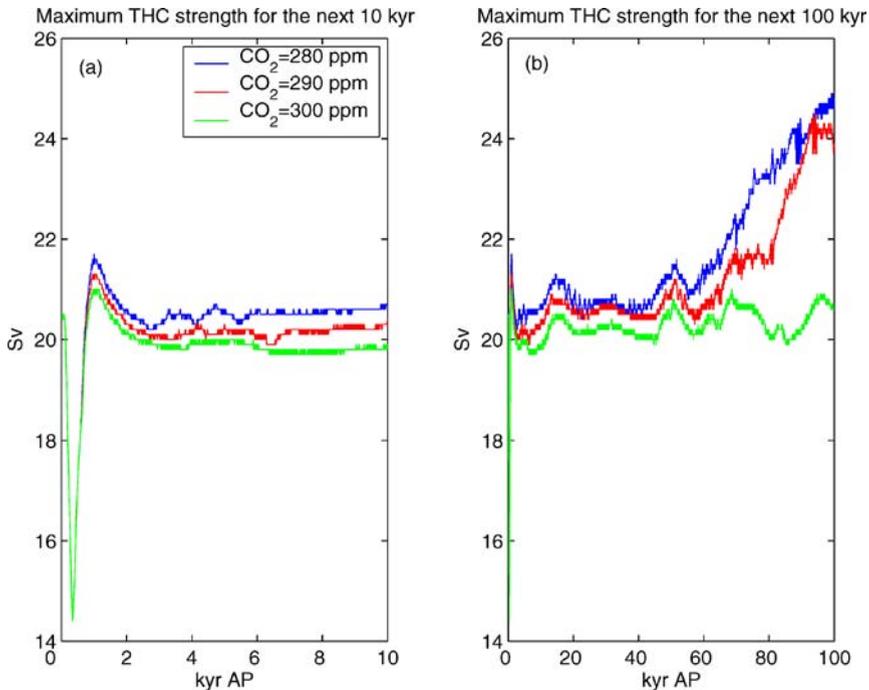
Fig. 9 Maximum THC intensity simulated by the green MPM with an initial global warming episode, followed by a constant CO_2 concentration of 280 ppm (blue), 290 ppm (red) and 300 ppm (green) after 1.2 kyr. The panel (a) represents the first 10 kyr of the run, and panel (b) represents the total 100 kyr of the run

After the glacial inception (for CO_2 levels of 280 and 290 ppm), the tree (desert) fraction has a slowly decreasing (increasing) trend due to the progressive cooling of the climate. We see also that, after the initial large-amplitude variations, the higher the CO_2 level, the higher the tree fraction and the lower the desert fraction.

The addition of the rapid initial change in the CO_2 forcing has triggered modifications of the early state of the climate system (THC strength, high latitude SAT, vegetation fraction). However, after a few millennia, the ice volume growth, maximum THC strength and vegetation fraction simulated under the three CO_2 levels with the initial warming episode superimposed (Figures 8, 9 and 10) are quite similar to the ones simulated under constant CO_2 without the initial warming episode (as seen on Figures 5, 6 and 7). Thus after a few millennia, the climate system has little memory of its initial or early conditions.

6 Conclusions

Projections for the next glacial inception were obtained from the orbitally forced green MPM which includes the vegetation-albedo feedback. Since the model does not include a global carbon cycle, different prescribed scenarios of atmospheric CO_2 concentration were also used as an external radiative forcing.

Experiments for the short-term future climate were run in order to determine if the green MPM was able to respond to an anthropogenic warming of the climate. Two global warming
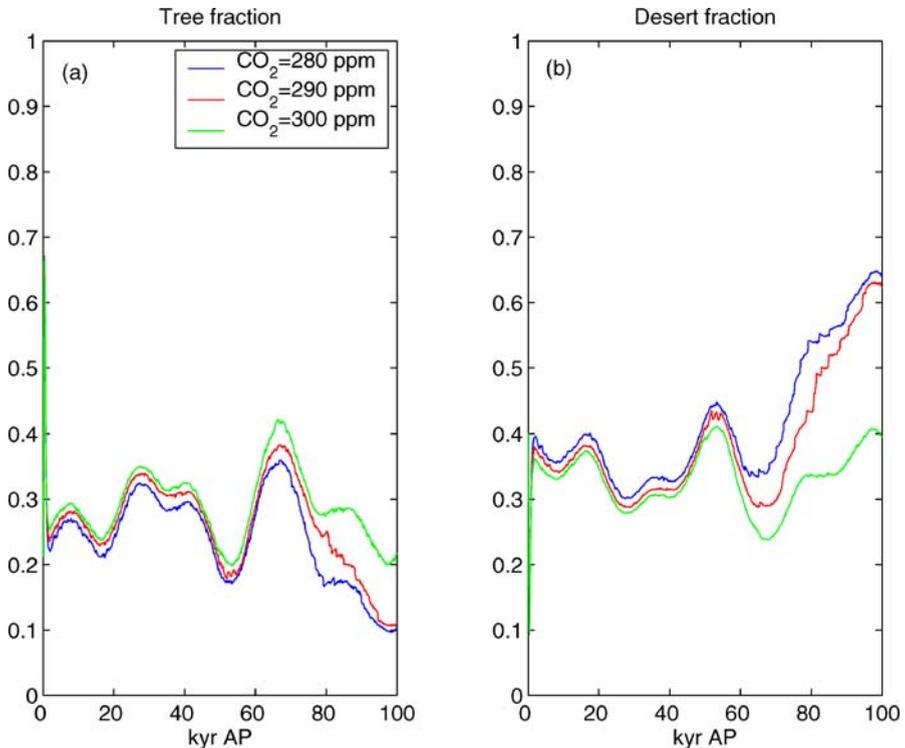
Fig. 10 Tree (a) and desert (b) fractions averaged between 60 and 75 °N simulated by the green MPM for the next 100 kyr, with an initial global warming episode followed by a constant CO_2 scenario of 280 ppm (blue), 290 ppm (red) and 300 ppm (green) after 1.2 kyr AP

scenarios were used: the first one represented a doubling of the CO_2 concentration (Petoukhov et al. 2005), and the second one was characterized by a large increase of the CO_2 level up to 1200 ppm in 2150, followed by a slow decrease over the next 1000 years (Rahmstorf and Ganopolski 1999). In both experiments the green MPM simulated a warm climate in response to the higher levels of CO_2, and the response for CO_2 doubling in particular, was found to lie in the range of GCMs run with similar forcing (Houghton et al. 2001).

The model was then run for the next 100 kyr, under prescribed CO_2 and orbital forcing, in order to determine the date of occurrence of a possible glacial inception. The evolution of the summer insolation at high northern latitudes for the next 100 kyr is quite exceptional and displays only weak variations. Thus the response of the green MPM is expected to be quite sensitive to the prescribed CO_2 level in the atmosphere. We first ran the model with constant CO_2 concentrations, ranging from 240 and 300 ppm. Three possible cases were found for the future evolution of the climate. A glacial inception is imminent for a CO_2 concentration between 240 and 270 ppm. For a CO_2 level between 280 and 290 ppm, the next glacial inception occurs in 50 kyr, which is similar to what was found by Loutre and Berger (2000). For a CO_2 concentration of 300 ppm or higher, no glacial inception occurs during the next 100 kyr. Before glacial inception occurs, the northern tree fraction has an evolution quite similar to that of the northern summer solar insolation; after the time of the glacial inception, the tree fraction progressively decreases due to the general cooling of the

climate. On the other hand, the maximum strength of the THC and the northern desert fraction have an evolution opposite in phase to that of the northern summer solar insolation; they both increase after the time of the glacial inception. The vegetation does not act as a driver of the glacial inception, but re-inforces the buildup of ice sheets and the cooling of the climate, through the vegetation-albedo feedback.

We next ran another series of 100-kyr experiments, but this time including a global warming episode during the first 1200 years of the run. We again observed a threshold for glaciation that depends on the CO_2 concentration. For CO_2 levels of 300 ppm or higher, a glacial inception would not occur in the next 100 kyr. Despite the initial modification of the climate system caused by the addition of the intense global warming episode at the beginning of the run, the evolution of the future climate is very similar to the one obtained with no initial global warming episode. The evolution of the tree fraction, desert fraction and THC intensity are similar to what was described above, with large initial variations superimposed. As an extension of our results, we note that if a very large anthropogenic release of carbon occurs (e.g., 5000 GtC), the impact on the atmospheric CO_2 level will be substantial and long-lasting: the concentration will remain above 400 ppm for over 300 kyr. Archer and Ganopolski (2005) show that in this case the CLIMBER-2 EMIC simulates an interglacial for the next 500 kyr.

While we believe our simulations shed new insights into the long-term evolution of the climate, we have to be somewhat cautious about our projections because of the limitations in the green MPM. However, the model is being continuously improved and these changes could be very beneficial for the study of future abrupt climate changes. Here we describe some of the current and future plans for improving the green MPM. First, we plan to add a global carbon cycle, so that, apart from anthropogenic releases of carbon, the atmospheric CO_2 concentration will not be prescribed, but will be calculated as an internal quantity in the model. Second, we plan to carry out future investigations with a global version of the green MPM, which has been recently developed (Wang 2005). We also plan to extend the ice sheet model to include a thermodynamic component. Finally, we wish to conduct future climate simulations with the global green MPM which includes, additionally, the vegetation-precipitation feedback (as modelled in Wang Y. et al. 2005c) and biogeochemical feedbacks (e.g., Archer et al. 2004).

References

Archer D, Ganopolski A (2005) A movable trigger: fossil fuel CO_2 and the onset of the next glaciation. Geochemistry Geophysics Geosystems 6:Q05003, doi:10.1029/2004GC000891

Archer D, Martin P, Buffett B, Brovkin V, Rahmstorf S, Ganopolski A (2004) The importance of ocean temperature to global biochemistry. Earth Planet Sci Lett 222:333–348

Beerling DJ, Woodward FI (2001) Vegetation and the terrestrial carbon cycle. Cambridge University Press, UK

Berger A (1978) Long-term variations of daily insolation and quaternary climatic changes. J Atmos Sci 35: 2362–2367

Berger A, Gallée H, Melice JL (1991) The Earth's future climate at the astronomical time scale. In: Goodess, CM, Palutikov JP (eds), Future climate change and radioactive waste disposal NIREX

Safety Series NSS/R257, Climatic Research Unit, University of East Anglia, Norwich, UK, pp 148–165

Berger A, Loutre MF (1996) Modelling the climate response to the astronomical and CO_2 forcings. Comptes rendus de l'academie des sciences de Paris t.323, serie IIa, 1–16

Berger A, Loutre MF, Gallée H (1996) Sensitivity of the LLN 2-D climate model to the astronomical and CO_2 forcing (from 200 kyr BP to 130 kyr AP). Scientific Report, Institut d'Astronomie et de Géophysique G. Lemaitre, Université catholique de Louvain 1996/1, 1–49

Berger A, Loutre MF, Tricot C (1993) Insolation and earth's orbital periods. J Geophys Res 98(D6): 10341–10362

Broecker WS (1998) The end of the present interglacial: how and when? Quaternary Science Reviews 17: 689–694

Brovkin V, Bendtsen J, Claussen M, Ganopolski A, Kubatzki C, Petoukhov V, Andreev A (2002) Carbon cycle, vegetation, and climate dynamics in the Holocene: experiments with the CLIMBER-2 model. Global Biogeochemical Cycles 16(4): 1139, doi: 10.1029/2001GB001662

Clark PU, Pollard D (1998) Origin of the middle Pleistocene transition by ice sheet erosion of regolith. Paleoceanography 13(1):1–9

Clark PU, Pisias NG, Stocker TF, Weaver AJ (2002) The role of the thermohaline circulation in abrupt climate change. Nature 415:863–869

Claussen et al. (2002) Earth system models of intermediate complexity: closing the gap in the spectrum of climate system models. Climate Dynamics 18(7):579–586

Cochelin A-S (2004) Simulation of glacial inceptions with the "green" McGill Paleoclimate Model. M.Sc. Thesis, McGill University. Available as C^2GCR Report No. 2004-2, McGill University, Montreal, Quebec, Canada, H3A 2K6

Cox PM, Betts RA, Bunton CB, Essery RLH, Rowntree PR, Smith J (1999) The impact of the new land surface physics on the GCM simulation of climate and climate sensitivity. Climate Dynamics 15:183–203

Dickinson RE, Henderson-Sellers A, Kennedy PJ (1993) Biosphere atmosphere transfer scheme (BATS) for the NCAR community climate model. Ncar tn387+str, NCAR Technical Note, National Center for Atmospheric Research, Boulder, Colorado, Climate and Global Dynamic Division

EPICA community members (2004) Eight glacial cycles from an Antarctic ice core. Nature 429:623–628

Heinrich H (1988) Origin and consequences of cyclic ice rafting in the northeast Atlantic Ocean during the past 130,000 years. Quat Res 29:142–152

Houghton JT, Ding Y, Griggs DJ, Noguer M, van der Linden PJ, Dai X, Maskell K, Johnson CA (eds) (2001) Climate change 2001: The scientific basis. contribution of working group i to the third assessment report of the intergovernmental panel on climate change. Cambridge University Press, Cambridge, United Kingdom and New York, USA, 881pp

Indermühle A, Stocker TF, Joos F, Fischer H, Smith HJ, Wahlen M, Deck B, Mastroianni D, Tschumi J, Blunier T, Meyer R, Stauffer B (1999) Holocene carbon-cycle dynamics based on CO_2 trapped in ice at Taylor Dome, Antarctica. Nature 398:121–126

Kukla GJ, Matthews RK, Mitchell MJ (1972) Present interglacial: how and when will it end? Quat Res 2:261–269

Le Treut H, McAvaney B (2000) A model intercomparison of equilibrium climate change in response to CO_2 doubling. Notes du Pole de Modelisation de l'IPSL, Institut Pierre Simon LaPlace, Paris, France No. 18

Letreguilly A, Huybrechts P, Reeh N (1991) Steady-state characteristics of the Greenland ice sheet under different climates. J Glaciol 37(125):149–157

Loutre MF (2003) Clues from MIS 11 to predict the future climate – a modelling point of view. Earth Planet Sci Lett 212:213–224

Loutre MF, Berger A (2000) Future climatic changes: are we entering an exceptionally long interglacial? Climatic Change 46:61–90

Manabe S, Spelman MJ, Bryan K (1991) Transient responses of a coupled ocean-atmosphere model to a gradual change of atmospheric CO_2. Part I: annual mean response. J Climate 4:785–818

Manabe S, Stouffer RJ (1994) Multiple-century response of a coupled ocean-atmosphere model to an increase of atmospheric carbon dioxide. J Climate 7:5–23

Marshall SJ, Clarke GKC (1997) A continuum mixture model of ice stream thermomechanics in the Laurentide ice sheet. 1. Theory. J Geophys Res 102:20599–20613

Milankovitch MM (1941) Canon of Insolation and the ice-age problem. Koniglich Serbische Akad. Belgrade, Yugoslavia

Oerlemans J, Van der Veen CJ (1984) Ice sheets and climate. Reidel Publishing. Dordrecht, 217pp

Petit JR, Jouzel J, Raynaud D, Barkov NI, Barnola JM, Basile I, Benders M, Chapellaz J, Davis M, Delaygue G, Delmotte M, Kotlyakov VM, Legrand M, Lipenkov VY, Lorius C, Pepin L, Ritz C, Saltzman E,

Stievenard M (1999) Climate and atmospheric history of the past 420,000 years from the Vostok ice core, Antarctica. Nature 399:429–436

Petoukhov V, Claussen M, Berger A, Crucifix M, Eby M, Eliseev AV, Fichefet T, Ganopolski A, Goosse H, Kamenkovich I, Mokhov I, Montoya M, Mysak LA, Sokolov A, Stone P, Wang Z, Weaver A (2005) EMIC intercomparison project (EMIP - CO$_2$): Comparative analysis of EMIC simulations of current climate and equilibrium and transient reponses to atmospheric CO$_2$ doubling. Climate Dynamics 25:363–385, doi: 10.1007/s00382-005-0042-3

Rahmstorf S, Ganopolski A (1999) Long-term global warming scenarios computed with an efficient coupled climate model. Climatic Change 43:353–367

Ruddiman WF (2001) Earth's climate: past and future. W.H. Freeman and Company, New York

Ruddiman WF (2003) Orbital insolation, ice volume and greenhouse gases. Quaternary Science Reviews 22:1597–1629

Saltzmann B, Maasch KA, Verbitsky MY (1993) Possible effects of anthropogenically-increased CO$_2$ on the dynamics of climate: implications for ice age cycles. Geophys Res Lett 20:1051–1054

Shackleton NJ, Opdyke ND (1976) Oxygen isotope and paleomagnetic stratigraphy of Pacific core V28-239, late Pliocene to latest Pleistocene. Mem Geol Soc Am 145:449–464

Vettoretti G, Peltier WR (2004) Sensitivity of glacial inception to orbital and greenhouse gas climate forcing. Quaternary Science Reviews 23(3–4):499–519

Wang Y, Mysak LA, Wang Z, Brovkin V (2005a) The greening of the McGill paleoclimate model. Part I: improved land surface scheme with vegetation dynamics. Climate Dynamics 24:469–480, doi: 10.1007/s00382-004-0515-9

Wang Y, Mysak LA, Wang Z, Brovkin V (2005b) The greening of the McGill paleoclimate model. Part II: simulation of Holocene millennial-scale natural climate changes. Climate Dynamics 24:481–496, doi: 10.1007/s00382-004-0516-8

Wang Y, Mysak LA, Roulet NT (2005c) Holocene climate and carbon cycle dynamics: experiments with the "green" McGill paleoclimate model. Global Biogeochemical Cycles 19:GB3022, doi: 10.1029/2005GB002484

Wang Z (2005) Two climatic states and feedbacks on thermohaline circulation in an Earth system model of intermediate complexity. Climate Dynamics 25:299–314, doi: 10.1007/s00382-005-0033-4

Wang Z, Mysak LA (2000) A simple coupled atmosphere-ocean-sea ice-land surface model for climate and paleoclimate studies. J Climate 13:1150–1172

Wang Z, Mysak LA (2002) Simulation of the last glacial inception and rapid ice sheet growth in the McGill Paleoclimate Model. Geophys Res Lett 29(23):2102, doi: 10.1029/2002GL015120

Wang Z, Hu R-M, Mysak LA, Blanchet J-P, Feng J (2004) A parameterization of solar energy disposition in the climate system. Atmosphere-Ocean 42(2):113–125

Wang Z, Cochelin A-SB, Mysak LA, Wang Y (2005) Simulation of the last glacial inception with the green McGill paleoclimate model. Geophys Res Lett 32:L12705 doi: 10.1029/2005GL023047

Wood RA, Vellinga M, Thorpe RB (2003) Global warming and thermohaline circulation stability. Phil. Trans R Soc London A361:1961–1975